Computational Materials Science 241 (2024) 113062

Contents lists available at ScienceDirect

Computational Materials Science

journal homepage: www.elsevier.com/locate/commatsci

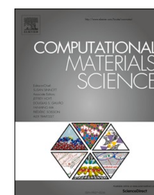

Full Length Article

Amorphous GaN: Polyamorphism and crystallization at high pressure

Murat Durandurdu

Department of Nanotechnology Engineering, Abdullah Gül University, Kayseri, Turkey

A R T I C L E I N F O

Keywords:
Gallium nitride
Amorphous
Polyamorphism

A B S T R A C T

Employing constant pressure ab initio simulations, we have shed light on the previously unknown high-pressure behavior of amorphous gallium nitride. Our findings reveal a two-step transformation sequence under pressure. The initial transition involves a polyamorphic transformation from a low-density amorphous (LDA) phase to a high-density amorphous (HDA) phase with an average coordination number of 5.4. Upon pressure release, the HDA state partially reverts to a denser amorphous network with a higher coordination number (4.34) compared to the original LDA phase. Further pressurization triggers the crystallization of the HDA state into a rocksalt structure. Remarkably, the electronic structure of the amorphous forms of GaN exhibits insignificant sensitivity to changes in coordination number, maintaining a band gap of approximately 1.7–2.0 eV across all phases.

1. Introduction

The crystalline form of gallium nitride (c-GaN) adopts a wurtzite (WZ) structure within the hexagonal crystal system polymorphs. Classified as a type III-V compound, c-GaN stands out as a prominent member of third-generation semiconductors, boasting exceptional properties like a wide band gap, excellent thermal conductivity and stability, and high electron mobility [1–6]. These properties translate into practical applications in areas like power electronics, with miniaturized, highly integrated devices offering enhanced power conversion efficiency, rapid switching speeds, and elevated power density [7,8]. Furthermore, GaN crystals pave the way for advancements in laser displays, smart grids, 5G communication, household lighting, and more.

Amorphous gallium nitride (a-GaN) emerges as a promising alternative to its crystalline counterpart. Extensive prior research has investigated the properties of a-GaN [9–16]. Compared to c-GaN, a-GaN may involve reduced processing costs due to potentially less stringent requirements [9]. Furthermore, its amorphous nature allows for deposition on a wider range of substrates and a unique capability to incorporate dopant atoms at higher concentrations compared to c-GaN [10]. This characteristic could lead to substantial modifications in the bandgap structure of a-GaN, paving the way for novel applications in optoelectronics distinct from those achievable with c-GaN [9,10].

Recent theoretical investigations employing advanced computational techniques have provided deeper insights into the atomic structure within a-GaN [17–21]. These studies have highlighted a chemically ordered structure with some inherent structural defects.

There has been considerable interest in understanding the high-pressure behavior of c-GaN as well. High-pressure experiments have revealed a WZ-to-Rocksalt (RS) phase transition in GaN between 37 and 52 GPa at room temperature [22–26]. Additionally, first-principles calculations at 0 K have predicted a transition to the RS phase at pressures ranging from 33 to 56 GPa [27–36], closely aligning with the experimental findings. However, the high-pressure behavior of its amorphous counterpart remains elusive. This discrepancy underscores a significant gap in our understanding. To address this gap, we propose a novel investigation utilizing constant-pressure ab initio calculations to shed light, for the first time, on the high-pressure behavior of a-GaN.

2. Method

In our research, we employed an ab initio approach based on density functional theory (DFT) to conduct high-pressure simulations on a-GaN [37]. We utilized the Troullier and Martins scheme [38] to construct pseudopotentials, incorporating the Ga 3d states into the core. The simulations were carried out under constant pressure within the isoenthalpic-isobaric (NPH) ensemble with the power quenching technique. Valence electrons were described using double zeta plus polarized (DZP) basis sets, and Brillouin zone integration was performed at the Γ point, employing the generalized gradient approximation (GGA) Perdew–Burke–Eruzerhof for solids (PBESol) functionals [39]. Pressure optimization was achieved using the Parrinello-Rahman method [40], with relaxation conducted till the maximum force was less than 0.01 eV/Å. The Hartree and exchange–correlation contributions to energy were determined with a mesh grid energy cut-off of 150 Ry.

For accurate band gap estimations in different phases of GaN, GGA +

E-mail address: murat.durandurdu@agu.edu.tr.

https://doi.org/10.1016/j.commatsci.2024.113062
Received 8 March 2024; Received in revised form 21 April 2024; Accepted 25 April 2024
Available online 1 May 2024
0927-0256/© 2024 Elsevier B.V. All rights reserved.

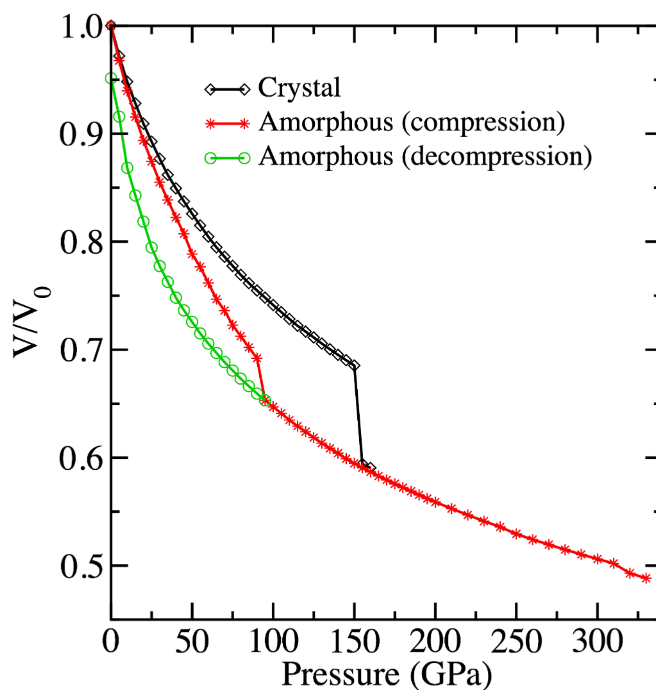

Fig. 1. Pressure-volume relation of crystalline and amorphous forms of GaN obtained using dynamical simulation. This plot highlights the distinct compressibility behaviors of the different phases. It is important to note that RS phase obtained directly from HDA phase through compression ultimately reaches a higher density than the RS phase derived from WZ-GaN at high pressures.

U calculations were performed. Hubbard potentials (U) were evaluated, particularly focusing on WZ-GaN, where the experimental band gap was found to be 3.26–3.41 eV [41–43]. Utilizing U = 8.25 eV for N-p state and U = 3.0 eV for Ga-p state, an approximate HOMO-LUMO band gap energy of 3.4 eV was obtained for WZ-GaN. These parameters were then applied consistently across all phases predicted to estimate their electronic structure.

Considering the structural resemblance between amorphous aluminum nitride (a-AlN) and a-GaN, an a-AlN model [44] was used to generate an a-GaN configuration. Following relaxation, the resulting model was found to be in good agreement with previous studies [18,21]. Visualization of the structures at the atomic level was facilitated using VESTA software [45], with further analysis carried out using the ISAACS program [46].

3. Results

3.1. c-GaN at high pressure

To ensure the reliability of our ab initio simulations for studying high-pressure behavior in GaN, we validated our chosen techniques and parameters by reproducing the well-characterized WZ-to-RS phase transformation at 155 GPa. Fig. 1 presents the equation of state for c-GaN, showing a gradual decrease in volume with increasing pressure followed by a sudden drop at 155 GPa, indicating a first-order phase transformation at this pressure. Symmetry analysis using the Phonopy code [47] confirms that the structure at this pressure exhibits $Fm\overline{3}m$ symmetry, with lattice parameters of $a = b = c = 3.868$ Å, and verifies the occurrence of the WZ-to-RS phase transformation at this pressure (see Fig. 2). This successful validation underscores the reliability of our simulation methods and parameters for further investigations.

It is noteworthy here that the transition pressure of 155 GPa observed in the dynamical simulation is significantly higher than the experimental results of 37–52 GPa. This discrepancy poses a primary challenge associated with the Parrinello-Rahman method. The overestimation in simulations suggests that there is an inherent energy barrier that the system needs to overcome for a solid phase to transform into another. Several inherent limitations in our simulation methodology contribute to this gap. Firstly, the use of periodic boundary conditions, while eliminating surface effects, can lead to an overestimation of transition pressures. Secondly, our simulations are inherently cleaner than real-world materials, as impurities often act as nucleation centers, lowering the required pressure for phase transitions. In the absence of these "seeds" for change in our simulations, the critical pressure may appear higher than it actually is. Lastly, the rapid pressurizing rates utilized in simulations may not allow sufficient time for the material to fully relax and rearrange, leading to the formation of "frozen states." In a real experiment with slower pressure changes, the material would have more time to adjust and transition at a lower pressure.

The thermodynamic theorem, however, does not account the potential presence of an activation barrier that separates the two structural phases. Consequently, as a subsequent step, we employ energy (E)-volume (V) calculations to investigate the stability of the WZ and RS phases. By fitting their energy-volume data (Fig. 3) to the third-order Birch-Murnaghan equation of state, we can determine the transition pressure where the enthalpy of the two phases becomes equivalent ($H = E_{tot} + PV$, with $P = -dE_{tot}/dV$ obtained through direct differentiation of the calculated energy-volume curves). The computed enthalpy curve of the WZ and RS states, presented in Fig. 3, allows us to determine a transition pressure of approximately 35 GPa. This finding aligns favorably with experimental and theoretical results falling within the range of 33–56 GPa [22–36].

3.2. a-GaN at high pressure

The equation of state of a-GaN is also depicted in Fig. 1. Similar to the crystalline form, the volume exhibits a gradual change, and at 95 GPa, a

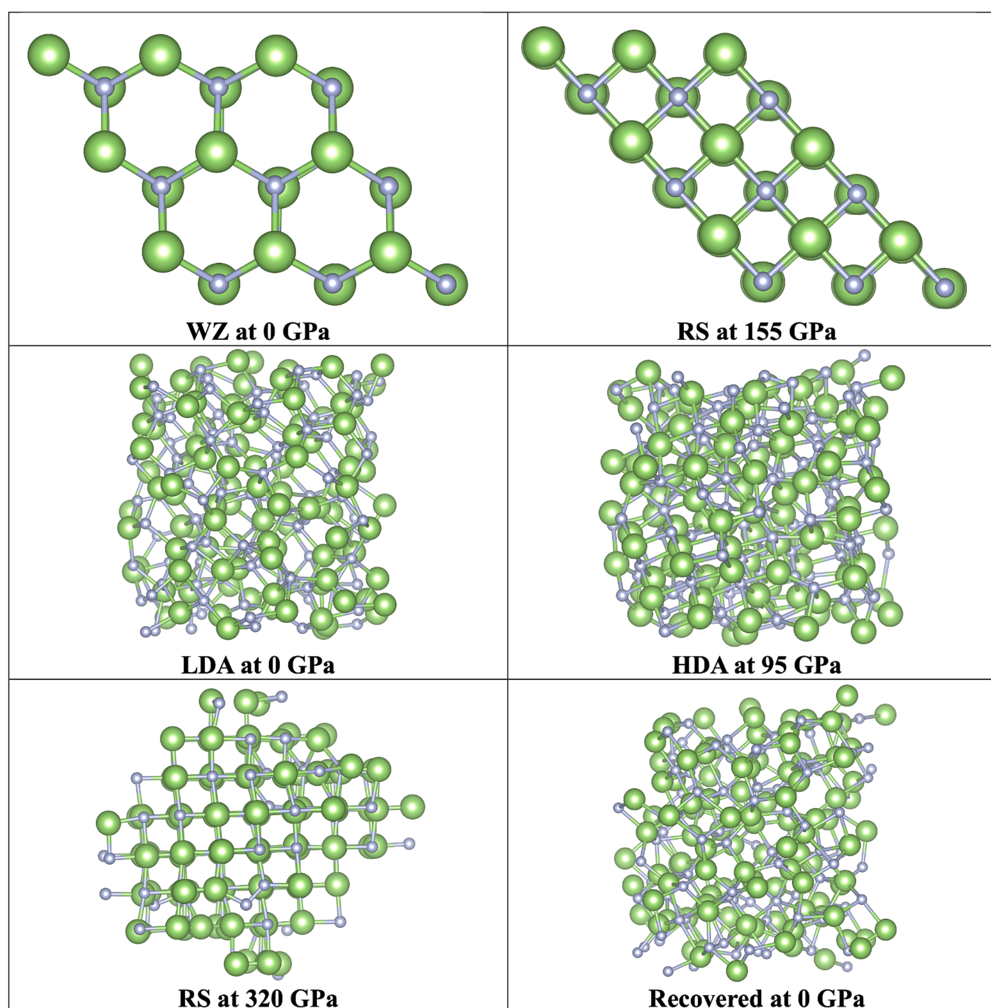

Fig. 2. Ball-stick representation of GaN phases at different pressures. This figure visually depicts the structural transformations of GaN under pressure.

noticeable volume collapse occurs, indicating a first-order phase change at this pressure. Further compression leads to a steady volume decrease until 320 GPa, followed by a minor additional collapse. Upon pressure release from 95 GPa, a hysteresis effect occurs: the volume partially recovers, but not entirely, suggesting a permanent densification in a-GaN.

To explore the structural changes induced by pressure, our investigation begins with analyzing the partial pair distribution functions (PPDFs) of the amorphous structure under various applied pressures. As depicted in Fig. 4, the PPDFs reveal the persistence of an amorphous network at 95 GPa, as evidenced by the absence of significant long-range correlations. This finding provides compelling evidence for a low-density amorphous (LDA) phase to high-density amorphous (HDA) phase transformation, known as *polyamorphism*, in GaN. The HDA state persists up to 320 GPa, where prominent peaks in the long-range correlations indicate pressure-induced ordering in the material. The visualization of the structure in Fig. 2 supports the crystallization at 320 GPa. However, analyzing the symmetry of this structure using Phonopy code proves challenging due to the presence of structural and coordination defects. Based on the observed high-pressure behavior of c-GaN, we hypothesize that this structure might resemble an imperfect RS structure, potentially exhibiting similar behavior under high pressure.

Given the typical correlation between pressure-induced amorphous-to-amorphous phase transitions and alterations in coordination numbers (CN) in nonmetallic systems, we undertook an investigation of CN as a function of pressure, illustrated in Fig. 5. At ambient condition, the CN of both Ga and N atoms in the LDA phase is 4.027 and about 90 % of Ga atoms and 95 % of N atoms present fourfold coordination. The remaining atoms are threefold and fivefold coordinated, in fairly agreement with the previous model [18]. With the application of pressure, CN initially experiences a minor increase until reaching 95 GPa, whereupon it sharply escalates to 5.4. Further compression leads to a gradual increase in CN with step-like increases at certain pressures before attaining a final value of 5.97 at 320 GPa. Analysis of the coordination distribution reveals that in the HDA state, approximately 43 % and 48 % of Ga atoms demonstrate fivefold and sixfold coordination, respectively, with the remainder primarily fourfold coordinated. Similarly, for N atoms, the percentages of fivefold and sixfold coordination are roughly 42 % and 46 %, correspondingly. Consequently, despite the phase transformation, some atoms retain tetrahedral coordination. At 320 GPa, the majority of atoms are sixfold coordinated, as expected.

Decompressing the model from 95 GPa reveals a persistent influence of the high-pressure phase on the structure. Although CN initially decreases slowly, a significant acceleration occurs below 25 GPa, ultimately leading to a final value of 4.34 for both Ga and N atoms at ambient pressure as depicted in Fig. 5. This significant observation suggests that the recovered model does not fully revert to its original state but instead retains signatures of the high-pressure motifs. Specifically, approximately 30 % of Ga and N atoms exhibit fivefold coordination, a characteristic of the high-pressure phase, in the recovered model, while 65 % remain fourfold coordinated, closer to the original state. These findings suggest that the pressure-induced transformation in a-GaN is *partially irreversible*. The recovered material exhibits a hybrid structure that combines elements of both the original and high-pressure phases.

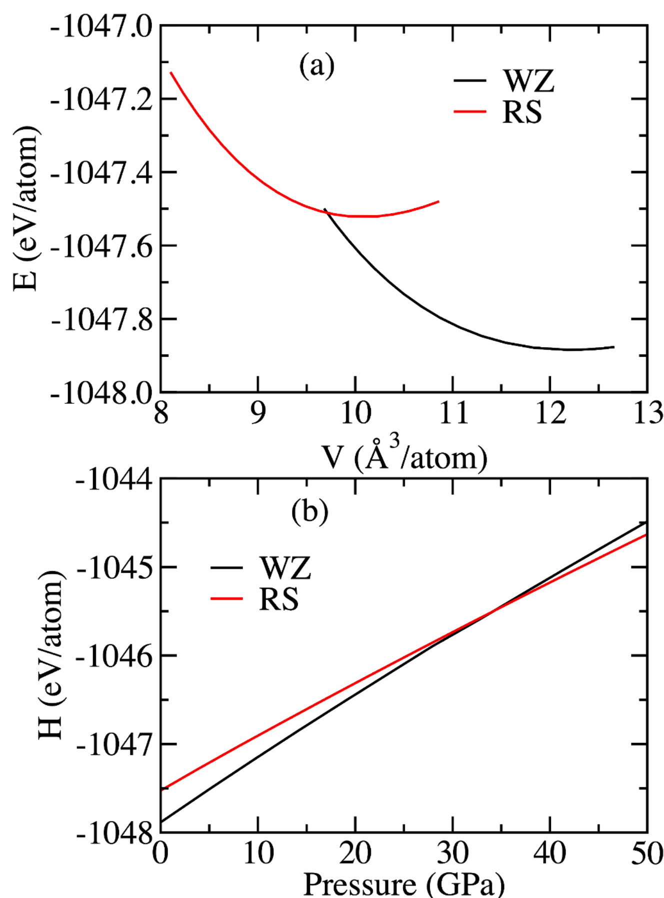

Fig. 3. The computed energies of WZ and RS phases are plotted as a function of volume (a) and the calculated enthalpies of WZ and RS structures are plotted as a function of pressure (b). The enthalpy curves of the WZ and RS phases intersect around 35 GPa, indicating a structural phase transition from the WZ to RS phase at this pressure.

The bond angle distribution functions (BADFs) illustrated in Fig. 6 offer valuable insights into the structural arrangement under pressure. Surprisingly, the analysis of the a-GaN model (LDA phase) yields unexpected results regarding its bond angle distribution. Contrary to the anticipated dominant peak around the ideal tetrahedral angle (109.47°) attributed to fourfold coordination, the observed distribution exhibits broad peaks with a main peak near the tetrahedral angle, consistent with previous findings [18]. Notably, the distribution also reveals unexpected subpeaks at angles around 88°–90° and wider angles, representing a significant deviation from the ideal tetrahedral configuration. These subpeaks suggest the presence of distinct local structural arrangements within the model. Similar observations have been made in other nitrogen-based amorphous models like $Al_xGa_{1-x}N$ and InN, attributed to the existence of edge-sharing units (fourfold rings) absent in their crystalline counterparts [20,48].

As pressure increases, the main peak undergoes a gradual shift towards lower angles, indicating a noticeable distortion within the system. Accompanied by the amorphous-to-amorphous phase transformation, the main peak relocates to approximately 90°. Further compression induces minimal changes due to the limited alteration in CN. However, at 320 GPa, the peaks at 90° and 180° become more pronounced, resembling the RS structure, suggesting intensified structural ordering. The distinct BADF of the recovered model suggests that the decompression process does not fully restore the original structure. The presence of the 90° peak indicates the persistence of structural features acquired during the high-pressure phase, even after returning to ambient pressure. This observation supports the notion of an irreversible amorphous-to-amorphous phase transformation as previously discussed.

We now turn our attention to the analysis of the electronic structure of some GaN phases. The computed electron density of states (EDOS) for specific phases, obtained through GGA + U calculations, is depicted in Fig. 7. For each phase, the Fermi level is shifted zero eV. Referring back to our methodology section, the HOMO-LUMO band gap of WZ-GaN is estimated to be approximately 3.4 eV, aligning well with experimental data ranging from 3.26 to 3.41 eV [41–43]. The LDA phase of GaN manifests a band gap energy of around 2.0 eV, while its HDA counterpart exhibits a slightly reduced value of 1.7 eV. Furthermore, the recovered amorphous phase presents a band gap of 1.86 eV. The predicted RS phase, on the other hand, demonstrates a band gap of about 1.76 eV. These findings imply that even significant variations in CN do not result in notable changes in the electronic structure of GaN in its amorphous states.

4. Discussion and conclusion

Computational simulations reveal a fascinating two-step transformation sequence in a-GaN subjected to increasing pressure. The process initiates with the LDA phase undergoing a first-order transition into a HDA phase. Subsequently, this HDA phase transforms further into a RS structure. While amorphous-to-amorphous transitions are commonplace in materials like ice, silicon, and various glasses [49–64], the observed first-order nature of the LDA-HDA transformation in GaN is exceptionally rare among amorphous compounds. Additionally, pressure-induced crystallization, as seen in a-GaN, is another uncommon

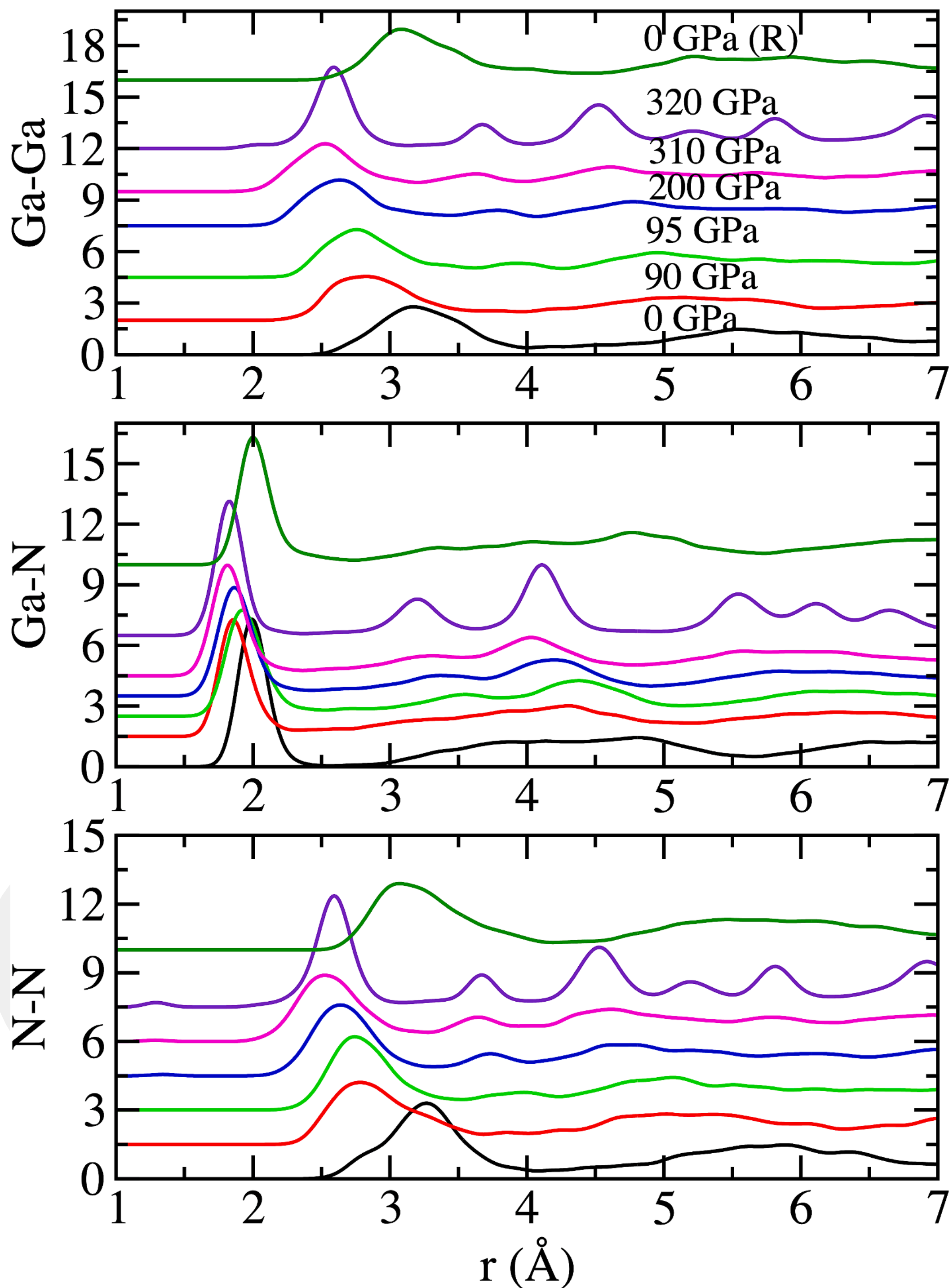

Fig. 4. Partial pair distribution functions (PPDFs) at selected pressures. The emergence of distinct peaks at 320 GPa signifies the development of long-range order within the material, indicating pressure-induced crystallization into the RS phase.

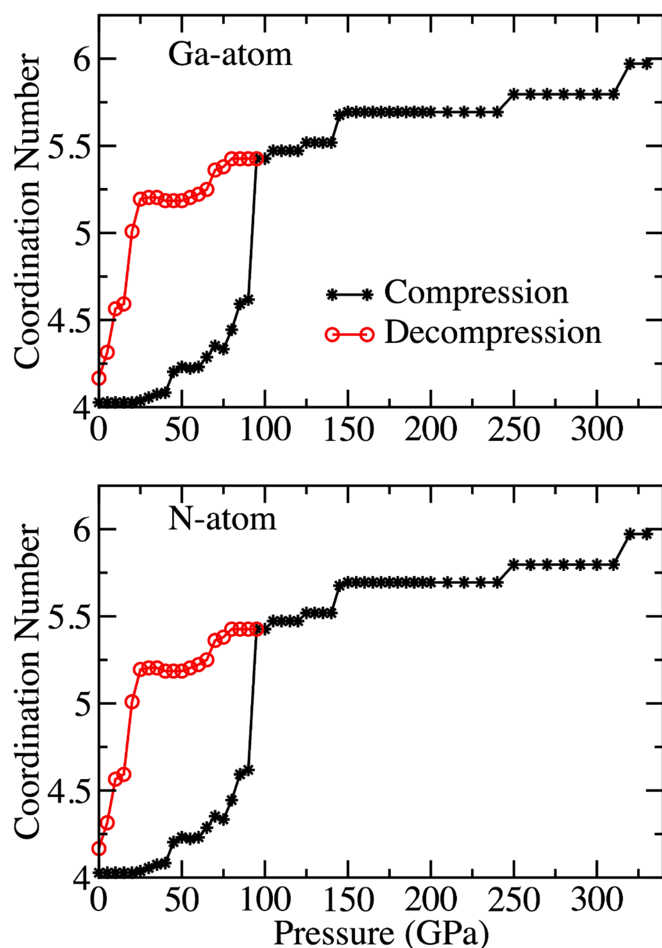

Fig. 5. Variation of coordination number (CN) as a function of pressure. This plot reveals a significant increase in CN upon transition from the LDA to HDA phase, followed by a decrease upon decompression. The incomplete recovery to the initial CN suggests partial irreversibility in the amorphous-to-amorphous transformation.

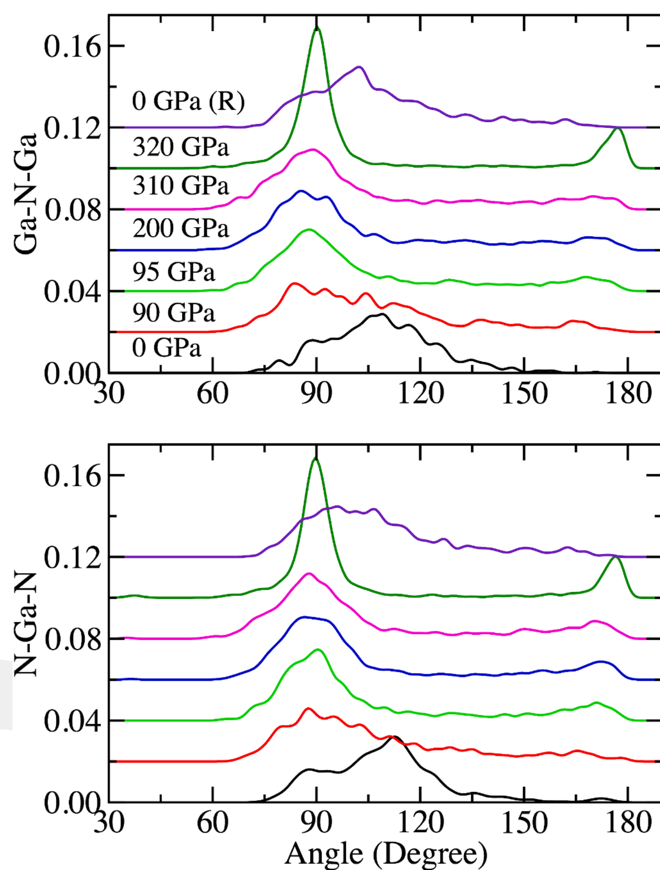

Fig. 6. Bond angle distribution function (BADF) at selected pressures. The broad peaks with a main peak near the tetrahedral angle and subpeaks at wider angles are characteristic of a-GaN. The shift in the main peak towards lower angles with increasing pressure indicates a distortion within the structure. Notably, the recovered phase retains a peak around 90°, suggesting the persistence of structural features acquired during the high-pressure transformation.

phenomenon in response to high-pressure treatments typically applied to amorphous materials [44,65,66]. This unique pressure sensitivity further underscores the distinct behavior of a-GaN.

Our simulations suggest that the LDA-HDA transition in a-GaN exhibits partial irreversibility, unlike the reversible transformations commonly observed in most amorphous compounds at ambient temperature. This behavior adds another layer of intrigue to a-GaN's response to pressure. However, it is crucial to acknowledge that the employed simulation technique, while successful in predicting various phase transformations, might have limitations. The observed partial irreversibility could potentially arise from these limitations, highlighting the need for further investigations, particularly experimental ones, to definitively confirm a-GaN's behavior under real-world pressure conditions.

Interestingly, the electronic structure of the amorphous forms of GaN appears relatively insensitive to changes in CN. Despite significant variations in CN among the LDA, HDA, and recovered phases, all exhibit a band gap of approximately 1.7–2.0 eV. This implies that over-coordinated motifs (having five or more bonds) do not significantly affect the electronic structure of a-GaN.

The Parrinello-Rahman technique used in our simulations is known to overestimate transition pressures. In the WZ-to-RS phase transformation, this overestimation ranges from 3 to 4.2 compared to experimental values of 37–52 GPa at room temperature. Therefore, a similar overestimation is expected for a-GaN. Consequently, we anticipate the actual LDA-HDA phase change in GaN to occur around 22 to 32 GPa in real-world conditions.

In conclusion, this study exposes remarkable pressure-induced transformations in a-GaN, characterized by a rare first-order amorphous-to-amorphous transition and subsequent crystallization. The observed partial irreversibility and pressure sensitivity further emphasize the unique response of a-GaN compared to other amorphous materials. Additionally, the electronic structure exhibits remarkable resilience to changes in CN, suggesting minimal impact on its fundamental properties. While acknowledging potential limitations of the simulation technique, this work paves the way for further exploration of this intriguing material and its response to external stimuli.

CRediT authorship contribution statement

Murat Durandurdu: Writing – review & editing, Writing – original draft, Visualization, Validation, Methodology, Investigation, Funding acquisition, Formal analysis, Conceptualization.

Declaration of competing interest

The authors declare that they have no known competing financial interests or personal relationships that could have appeared to influence the work reported in this paper.

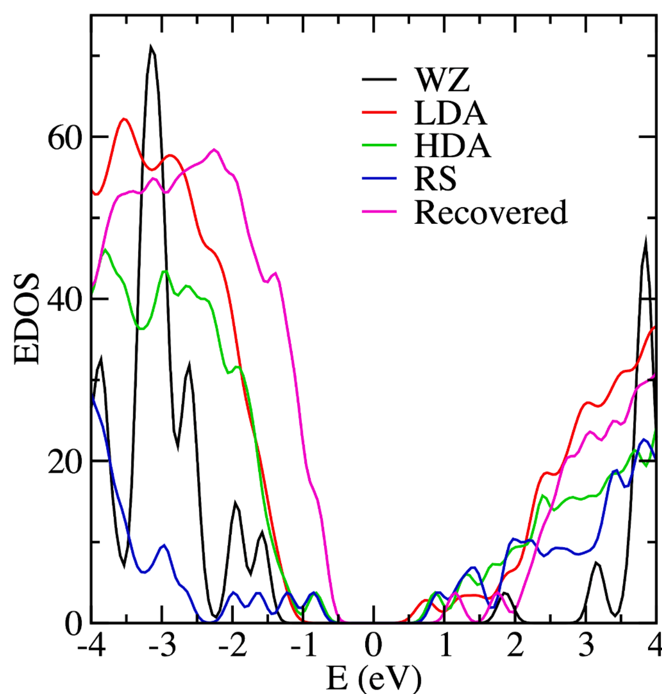

Fig. 7. Electron density of states of some GaN phases. This plot depicts the band gap of various GaN phases, as calculated using GGA + U methods. Interestingly, the band gap exhibits minimal variation across the amorphous phases (LDA, HDA, recovered) despite significant changes in coordination number.

Data availability

Data will be made available on request.

Acknowledgments

The author expresses gratitude for the support provided by the Abdullah Gül University Support Foundation. Additionally, the author acknowledges the computing resources and time generously provided by TÜBİTAK ULAKBİM High Performance and Grid Computing Center (TRUBA resources).

References:

[1] Y. Ren, Z.Y. He, B. Dong, C.G. Wanga, Z.H. Zenga, Q.X. Lia, Z.T. Chena, L.A. Lic, N. Y. Liu, Analysis of electrical properties in Ni/GaN schottky contacts on nonpolar/semipolar GaN free-standing substrates, J. Alloys Compd. 898 (2022) 162817–162822.
[2] S. Kotzea, A. Debald, M. Heuken, H. Kalisch, A. Vescan, High-mobility GaN-on-sapphire pn diodes with near-unity ideality factor and large breakdown voltage, J. Phys. d: Appl. Phys. 52 (2019) 285101.
[3] R.X. Yu, G.D. Wang, Y.L. Shao, Y.Z. Wu, S.Z. Wang, G. Lian, B.G. Zhang, H.X. Hu, L. Liu, L. Zhang, From bulk to porous GaN crystal: precise structural control and its application in ultraviolet photodetectors, J. Mater. Chem. C 7 (2019) 14116–14122.
[4] Q. Li, J. Yu, S. Wang, G. Wang, G. Liu, L. Liu, S. Zhang, X. Xu, L. Zhang, Research progress in the postprocessing and application of GaN crystal, CrystEngComm 25 (2023) 715–725.
[5] Q.B. Li, G.X. Liu, J.X. Yu, G.D. Wang, S.Z. Wang, T. Cheng, C.M. Chen, L. Liu, J.-Y. Yang, X.G. Xu, L. Zhang, A perovskite/porous GaN crystal hybrid structure for ultrahigh sensitivity ultraviolet photodetectors, J. Mater. Chem. C 10 (2022) 8321–8328.
[6] I. Susanto, K.-Y. Kan, I.-S. Yu, Temperature effects for GaN films grown on 4H-SiC substrate with 4 miscutting orientation by plasma-assisted molecular beam epitaxy, J. Alloys Compd. 723 (2017) 21–29.
[7] K.J. Singh, Y.-M. Huang, T. Ahmed, A.-C. Liu, S.-W.-H. Chen, F.-J. Liou, T.Z. Wu, C.-C. Lin, C.-W. Chow, G.-R. Lin, H.-C. Kuo, Improved Optical and Electrical Characteristics of GaN-Based Micro-LEDs by Optimized Sidewall Passivation, Appl. Sci. 10 (2020) 7384–7390.
[8] B.N. Pushpakaran, A.S. Subburaj, S.B. Bayne, Commercial GaN-based power electronic systems: A review, J. Electron. Mater. 49 (2020) 6247–6262.
[9] S.H. Shim, K.B. Shim, J. Yoon, Y. Shimizu, T. Sasaki, N., Koshizaki Blue luminescence from amorphous GaN films deposited by pulsed-laser ablation at room temperature.", Thin Solid Films 472 (2005) 11–15.
[10] X. Pan, Z. Zhang, L. Jia, H. Li, E. Xie, Room temperature visible green luminescence from a-GaN: Er film deposited by DC magnetron sputtering, J. Alloys Compd. 458 (2008) 579–582.
[11] T. Hariu, T. Usuba, H. Adachi, Y. Shibata, Reactive sputtering of gallium nitride thin films for GaAs MIS structures, Appl. Phys. Lett. 32 (1978) 252–254.
[12] H.J. Trodahl, F. Budde, B.J. Ruck, S. Granville, A. Koo, A. Bittar, Raman spectroscopy of nanocrystalline and amorphous GaN, J. Appl. Phys. 97 (2005) 084309–084313.
[13] Z. Hassan, Y.C. Lee, F.K. Yam, K. Ibrahim, M.E. Kordesch, W. Halverson, P. C. Colter, Characteristics of low-temperature-grown GaN films on Si (111), Solid State Commun. 133 (2005) 283–287.
[14] J. Kennedy, A. Markwitz, H.J. Trodahl, B.J. Ruck, S.M. Durbin, W. Gao, Ion beam analysis of amorphous and nanocrystalline group III-V nitride and ZnO thin films, J. Electron. Mater. 36 (2007) 472–482.
[15] A. Al-Zouhbi, N.S. Al-Din, Structural and optoelectronic properties of amorphous GaN thin films, Opt. Rev. 15 (2008) 251–254.
[16] A. Bittar, H.J. Trodahl, N.T. Kemp, A. Markwitz, Ion-assisted deposition of amorphous GaN: Raman and optical properties, Appl. Phys. Lett. 78 (2001) 619–621.
[17] P. Stumm, D.A. Drabold, Can amorphous GaN serve as a useful electronic material? Phys. Rev. Lett. 79 (1997) 677–680.
[18] B. Cai, D.A. Drabold, Properties of amorphous GaN from first-principles simulations, Phys. Rev. B 84 (2011) 075216–075221.
[19] M. Yu, D.A. Drabold, Density dependence of the structural and electronic properties of amorphous GaN, Solid State Commun. 108 (1998) 413–447.
[20] K. Chen, D.A. Drabold, First principles molecular dynamics study of amorphous AlxGa1− xN alloys, J. Appl. Phys. 91 (2002) 9743–9751.
[21] S.P. Tamariz-Kaufmann, A.A. Valladares, A. Valladares, R.M. Valladares, First-principles calculation of the electronic and topological properties of crystalline and amorphous AlxGa1− xN, J. Non-Cryst. Solids 420 (2015) 7–11.
[22] H. Xia, Q. Xia, A.L. Ruoff, High-pressure structure of gallium nitride: Wurtzite-to-rocksalt phase transition, Phys. Rev. B 47 (1993) 12925–12928.
[23] M. Ueno, M. Yoshida, A. Onodera, O. Shimomura, K. Takemura, Stability of the wurtzite-type structure under high pressure: GaN and InN, Phys. Rev. B 49 (1994) 14–21.
[24] P. Perlin, C. Jauberthie-Carillon, J.P. Itie, A. San Miguel, I. Grzegory, A. Polian, Raman scattering and x-ray-absorption spectroscopy in gallium nitride under high pressure, Phys. Rev. B 45 (1992) 83–89.
[25] M.P. Halsall, P. Harmer, P.J. Parbrook, S.J. Henley, Raman scattering and absorption study of the high-pressure wurtzite to rocksalt phase transition of GaN, Phys. Rev. B 69 (2004) 235207–235211.
[26] B. Sadovyi, M. Wierzbowska, S. Stelmakh, S. Boccato, S. Gierlotka, T. Irifune, S. Porowski, I. Grzegory, Experimental and theoretical evidence of the temperature-induced wurtzite to rocksalt phase transition in GaN under high pressure, Phys. Rev. B 102 (2020) 235109–235117.
[27] A.M. Saitta, F. Decremps, Unifying description of the wurtzite-to-rocksalt phase transition in wide-gap semiconductors: The effect of d electrons on the elastic constants, Phys. Rev. B 70 (2004) 035214–035218.
[28] F.S. Saoud, J.C. Plenet, L. Louail, D. Maouche, Mechanism of the phase transition in GaN under pressure up to 100 GPa, Comput. Theor. Chem. 964 (2011) 65–71.
[29] N.E. Christensen, I. Gorczyca, Optical and structural properties of III-V nitrides under pressure, Phys. Rev. B 50 (1994) 4397–4415.
[30] A. Muñoz, K. Kunc, New phases and physical properties of the semiconducting nitrides: AlN, GaN, InN, Comput. Mater. Sci. 2 (1994) 400–412.
[31] J. Cai, N.X. Chen, Microscopic mechanism of the wurtzite-to-rocksalt phase transition of the group-III nitrides from first principles, Phys. Rev. B 75 (2007), 134109134120.
[32] M. Abu-Jafar, A.I. Al-Sharif, A. Qteish, FP-LAPW and pseudopotential calculations of the structural phase transformations of GaN under high-pressure, Solid State Commun. 116 (2000) 389–393.
[33] R. Pandey, N.M. Harrison, M. Seel, The high-pressure phase transitions of silicon and gallium nitride: A comparative study of Hartree-Fock and density functional calculations, J. Phys.: Condens. Matter 8 (1996) 3993–4000.
[34] J. Serrano, A. Rubio, E. Hernández, A. Muñoz, A. Mujica, Theoretical study of the relative stability of structural phases in group-III nitrides at high pressures, Phys. Rev. B 62 (2000) 16612–16623.
[35] A. Mujica, A. Rubio, A. Munoz, R.J. Needs, High-pressure phases of group-IV, III–V, and II–VI compounds, Rev. Mod. Phys. 75 (2003) 863–912.
[36] C. Soykan, Ab-initio Calculations of the Physical Properties in Gallium Nitride at Equilibrium Phases: Rocksalt and Wurtzite, Süleyman Demirel Üniversitesi Fen Bilimleri Enstitüsü Dergisi 22 (2018) 13–23.
[37] J.M. Soler, et al., The SIESTA method for ab initio order-N materials simulation, J. Phys. Condens. Matter 14 (2002) 2745.
[38] N. Troullier, J.L. Martins, Efficient pseudopotentials for plane-wave calculations, Phys. Rev. B 43 (1991) 1993–2006.
[39] J.P. Perdew, et al., Restoring the density-gradient expansion for exchange in solids and surfaces, Phys. Rev. Lett. 100 (2008) 136406–136409.
[40] M. Parrinello, A. Rahman, Polymorphic transitions in single crystals: A new molecular dynamics method, J. Appl. Phys. 52 (1981) 7182–7190.
[41] E. Kauer, A. Rabenau, Über den Bandabstand von Galliumnitrid und Aluminiumnitrid, Z. Naturforsch. A 12 (1957) 942.
[42] H. Pi Maruska, J.J. Tietjen, The preparation and properties of vapor-deposited single-crystal-line GaN, Appl. Phys. Lett. 15 (1969) 327–329.

[43] R.C. Powell, N.-E. Lee, Y.-W. Kim, J.E. Greene, Heteroepitaxial wurtzite and zinc-blende structure GaN grown by reactive-ion molecular-beam epitaxy: Growth kinetics, microstructure, and properties, J. Appl. Phys. 73 (1993) 189–204.
[44] M. Durandurdu, Polyamorphism in aluminum nitride: A first principles molecular dynamics study, J. Am. Ceram. Soc. 99 (2016) 1594–1600.
[45] K. Momma, F. Izumi, VESTA 3 for three-dimensional visualization of crystal, volumetric and morphology data, J. Appl. Crystallogr. 44 (2011) 1272–1276.
[46] S. Le Roux, V. Petkov, ISAACS–interactive structure analysis of amorphous and crystalline systems, J. Appl. Crystallogr. 43 (2010) 81–85.
[47] S. Togo, I. Tanaka, First principles phonon calculations in materials science, Scripta Materialia 108 (2015) 1–5.
[48] B. Cai, D.A. Drabold, Ab initio models of amorphous InN, Phys. Rev. B 79 (2009) 195204–195207.
[49] O. Mishima, L.D. Calvert, E. Whalley, An apparently first-order transition between two amorphous phases of ice induced by pressure, Nature 314 (1985) 76–78.
[50] R. Martonak, D. Donadio, M. Parrinello, Evolution of the structure of amorphous ice: From low-density amorphous through high-density amorphous to very high-density amorphous ice, J. Chem. Phys. 122 (2005) 134501–134504.
[51] M. Durandurdu, D.A. Drabold, Ab initio simulation of first-order amorphous-to-amorphous phase transition of silicon, Phys. Rev. B 64 (2001) 014101–014107.
[52] S.K. Deb, M. Wilding, M. Somayazulu, et al., Pressure-induced amorphization and an amorphous–amorphous transition in densified porous silicon, Nature 414 (2001) 528–530.
[53] P.F. McMillan, M. Wilson, D. Daisenberger, et al., A density-driven phase transition between semiconducting and metallic polyamorphs of silicon, Nat. Mater. 4 (2005) 680–684.
[54] V.L. Deringer, N. Bernstein, G. Csa ́nyi, et al., Origins of structural and electronic transitions in disordered silicon, Nature 589 (2021) 59–64.
[55] E. Principi, F. Decremps, A. Di Cicco, et al., Pressure induced phase transitions in amorphous Ge, Phys. Scr. T115 (2005) 381–383.
[56] M. Durandurdu, D.A. Drabold, First-order pressure-induced polyamorphism in germanium, Phys. Rev. B 66 (2002) 041201–041204.
[57] N. Li, R. Sakidja, S. Aryal, et al., Densification of a continuous random network model of amorphous SiO2 glass, Phys. Chem. Chem. Phys. 16 (2014) 1500–1514.
[58] M. Guerette, M.R. Ackerson, J. Thomas, et al., Structure and properties of silica glass densified in cold compression and hot compression, Sci Rep. 5, Article number 15343 (2015).
[59] A. Zeidler, K. Wezka, R.F. Rowlands, et al., High-pressure transformation of SiO2 glass from a tetrahedral to an octahedral network: A joint approach using neutron diffraction and molecular dynamics, Phys. Rev. Lett. 113 (2014) 135501–135505.
[60] O.B. Tsiok, V.V. Brazhkin, A.G. Lyapin, et al., Logarithmic kinetics of the amorphous-amorphous transformations in SiO2 and GeO2 glasses under high pressure, Phys. Rev. Lett. 80 (1998) 999–1002.
[61] P.S. Salmon, J.W. Drewitt, D.A. Whittaker, et al., Density-driven structural transformations in network forming glasses: a high-pressure neutron diffraction study of GeO2 glass up to 17.5 GPa, J. Phys. Condens Matter. 24 (2012) 415102–415117.
[62] V.V. Brazhkin, E. Bychkov, O.B. Tsiok, Direct volumetric study of high-pressure driven polyamorphism and relaxation in the glassy germanium chalcogenides, J. Phys. Chem. B 120 (2016) 358–363.
[63] L. Properzi, A. Di Cicco, L. Nataf, et al., Short-range order of compressed amorphous GeSe2, Sci Rep. 5, Article number 10188 (2015).
[64] L. Properzi, M. Santoro, M. Minicucci, et al., Structural evolution mechanisms of amorphous and liquid As2Se3 at high pressures, Phys. Rev. B 93 (2016) 214205–214212.
[65] M. Xu, Y. Meng, Y.Q. Cheng, et al., Pressure-induced crystallization of amorphous Ge2Sb2Te5, J. Appl. Phys. 108 (2010) 083519–083523.
[66] M. Wu, S.T. John, S.Y. Wang, C.Z. Wang, J.Z. Jiang, Origin of pressure-induced crystallization of Ce75Al25 metallic glass, Nat. Commun. 6 (2015) 6493–6649.

GCRIS